A mechanistic Study of the electrochemical reaction between nitrostyrene and benzaldehyde; DFT calculations on all possible routes and intermediates

Donya Shirvani
Isfahan University of Technology
Hossein Tavakol
h_tavakol@iut.ac.ir

Isfahan University of Technology
Mahshid Abedini
Isfahan University of Technology

Research Article

Keywords: β-nitrostyrene, Computational, Electrochemistry, Mechanism

Posted Date: July 29th, 2024

DOI: https://doi.org/10.21203/rs.3.rs-4684231/v1

Additional Declarations: No competing interests reported.

Version of Record: A version of this preprint was published at Research on Chemical Intermediates on August 24th, 2024. See the published version at https://doi.org/10.1007/s11164-024-05382-7.

Abstract

A theoretical investigation of electrochemical reaction between β-nitrostyrene and benzaldehyde was conducted at the DFT M06-2X/def2-TZVP level of theory. The reaction mechanism was dissected into five proposed routes, via 3 pathways, concluding to 4 possible products (P1 to P4). To gain a comprehensive understanding, we explored these routes both in the gas phase and in solution using three solvents: dimethylformamide, methanol, and water. In the gas phase, the overall barriers of these five routes (the energy in parentheses refers to the relative G versus reactants in kcal/mol) are in this order: A2 (-48.22) < A1 (21.29) < C1 (21.59) < B (29.81) < C2 (77.59). The ΔG for the formation of four products (the energy in parentheses refers to the relative G versus reactants in kcal/mol) are in this order: P2 (-233.40) < P4 (-82.13) < P3 (-74.18) < P1 (-46.97). Therefore, in the extra amount of both benzaldehyde and proton, P2 is the major product, in the extra amount of benzaldehyde and minimum amount of proton, P1 is preferred, and in the small amount of benzaldehyde and proton, P4 is preferred (only via C1 route). In the solvents, despite the gas phase data, path B and product P3 are a favorable path and product. Thermodynamically, the average relative G in three solvents for P3 is -112.09 kcal/mol, for P2 is -112.1, for P4 is -118.46, and for P1 is -60.25. Kinetically, the average relative G in three solvents for the transition states of P3 is -8.25 kcal/mol, P2 is -42.84, P4 is 34.16 via route C1 and 29.05 via route C2, and P1 is 95.81. Therefore, in the excess concentration of proton, P2 is the most favorable product by both kinetic and thermodynamic data and the for P low concentration of proton, P3 is the most favorable product.

1.Introduction

The exploration of electrochemical properties at the molecular level has become increasingly pivotal in advancing our understanding of chemical reactions [1]. Among the various compounds of interest, β-Nitrostyrene is particularly noteworthy for its distinctive electronic configuration and reactivity[2]. β-Nitrostyrene is an α,β-unsaturated compound from the class of nitroolefins characterized by the presence of a nitro group attached to a styrene scaffold, which showcases a diverse range of chemical reactions and has many applications in the field of synthesis of organic compounds [3–5]. Chemically, The synthesis of β-Nitrostyrene can be achieved through the Henry reaction of benzaldehyde and nitromethane [6, 7] or by direct nitration of styrene using nitric oxide [8]. This compound also has anti-cancer, anti-bacterial and anti-fungal properties, which are among the characteristics of their significant [9–11]. This multifaceted compound can undergo a variety of reactions. It is a common substrate for Michael addition reactions [12–14]. It can also engage in [3 + 2] and [4 + 2] cycloaddition reactions, which are useful for creating five-membered [15] and six-membered rings [16], respectively. Upon treatment with halogens, β-nitrostyrenes can form halogenated derivatives [17–19]. In addition, it can be reduced to form amines, which are key intermediates in the synthesis of many pharmaceuticals [20–22]. Besides, Recent studies have shown that β-nitrostyrene can undergo Michael addition with diethyl malonate in the presence of Organocatalysts like bispidines [23].

Computational chemistry seeks to simulate and understand the properties of molecules and their reactions. Techniques such as density functional theory (DFT), molecular dynamics (MD), and ab initio methods allow scientists to explore molecular landscapes beyond the laboratory limitations [24–26]. These methods have been instrumental in predicting reaction outcomes, designing new materials, and even drug discovery [27]. Moreover, they are proficient in understanding and predicting the behavior of pollutants and their impact on the environment [28]. They can also be used to design and optimize catalysts that are crucial for speeding up chemical reactions [29]. Several cases of theoretical and computational research on beta-nitrostyrene compounds have been conducted. In a study conducted by Jiang et al., the asymmetric conjugate addition of dimethylmalonate to β-nitrostyrene, facilitated by cinchona alkaloid QD-4 as an organic catalyst, was examined. The team employed density functional theory and ab initio methods to explore the reaction's mechanism and its enantioselectivity [30]. In another research, Kula and Zawadzińska delved into the regioselectivity of [3 + 2] cycloaddition reactions, pairing benzonitrile N-oxide with two sets of para-substituted β-nitrostyrene analogues, using molecular electron density theory. In the mentioned investigation, the B3LYP method and a 6-31G(d) basis set was utilized for quantum calculations[31]. Furthermore, Gan et al. investigated on the asymmetric Michael reaction between aldehydes and nitrostyrene, catalyzed by a novel (S)-tertbutyl-diphenyl-silyl-pyrrolidine catalyst, applying the density functional theory (DFT) at the B3LYP/6-311G** level [32]. Wang embarked on a computational analysis of the Michael addition reaction of aldehydes to nitrostyrene in the presence of a proline-derived catalyst in aqueous conditions. Molecular dynamics (MD) simulations was applied to examine the emulsion structure, focusing on the influence of the catalyst's structure [33].

Computational electrochemistry extends all computational chemistry principles to the realm of redox chemistry, where electron transfer is paramount [34, 35]. By simulating electrochemical cells and interfaces, researchers can predict redox potentials, study corrosion mechanisms, and design better batteries and fuel cells [36–38]. Computational electrochemistry specifically deals with the challenges and phenomena associated with electron transfer processes [39]. β-Nitrostyrene, a molecule of significant synthetic utility, serves as an ideal candidate for computational electrochemical studies due to its electroactive nature and structural features that influence electron distribution. The presence of the nitro group adjacent to the vinyl group significantly alters the molecule's electron density in nitro vinyl part, thereby influencing its electrochemical characteristics [40].

The electrochemical reaction between benzaldehyde and β-Nitrostyrene is of particular interest due to the unique reactivity of these compounds. This article delves into a comprehensive computational study of radical anions in β-Nitrostyrene and benzaldehyde, two compounds of considerable interest due to their widespread applications and intriguing chemical properties

While numerous studies have been conducted on these compounds, our research stands out by providing new and superior information. Through this work and based on the previous experiences of this group on the DFT study of the reaction mechanisms and chemical processes [41–44], by employing

advanced simulation techniques we aim to bridge the gap between theory and experiment, providing valuable predictions that can guide future experimental studies.

2. Computational details

The computational investigation of β-Nitrostyrene was conducted using a multi-tiered approach to ensure the accuracy and reliability of the results. The initial geometries of the molecules were first pre-optimized using the B3LYP functional with the 6-31G basis set. This level of theory is widely recognized for its balance between computational cost and accuracy in predicting molecular structures and energies [45]. The B3LYP functional, which combines Becke's three-parameter exchange functional with the Lee-Yang-Parr correlation functional, is particularly adept at handling systems with extensive π-conjugation and The 6-31G(d) basis set was chosen for its proven effectiveness in providing a good representation of the electron distribution within organic molecules while maintaining computational efficiency [46, 47]. For the next and final geometry optimization and other calculations, the M06-2X method with the Def2TZVP basis set was employed. The M06-2X functional is a highly parameterized, range-separated hybrid functional designed for a broad spectrum of applications, including main group and transition metal chemistry, as well as noncovalent interactions [48]. The Def2TZVP basis set provides a comprehensive description of the valence electrons, which is crucial for accurate electrochemical predictions [49].

All calculations were performed using the Gaussian 09W suite of program package [50], which is well-suited for a wide range of computational chemistry applications. The choice of software ensures that the computational procedures are robust and the results are reproducible. The resulting data were analyzed using GaussView 6 software to visualize molecular orbitals, electron density distributions, and to perform topological analyses of the electron density. These tools facilitated a deeper understanding of the electronic factors influencing the reactivity of β-Nitrostyrene. Solvent effects were examined employing PCM model (SCRF keyword) using three different solvents, DMF, methanol and water.

3. Results and discussion

3.1. Describing the possible reaction pathways

Considering the importance of β-nitrostyrene synthesis and the possibility of its electrochemical reaction with benzaldehyde, the theoretical investigation of this reaction was included in the agenda of this research. Since the studied reaction is electrochemical, it was assumed that its initiator is an electron which is taken by β-nitrostyrene from the electrode placed in the electrochemical cell that turns this compound into a radical anion. By examining different routes, ultimately five main routes, which were more likely to occur than the others were reached. The aim of this research is to theoretically investigate the possible electrochemical reactions of β-nitrostyrene. In this regard, all species, intermediates, and potential products resulting from the radicalization of the starting material, dimerization, and reaction of β-nitrostyrene with benzaldehyde were examined.

After drawing the molecules in each path, the optimal structure of each of these species was determined by calculations. Then, the optimized species were analyzed from several aspects, including energy, geometric parameters, natural bond orbital (NBO) charges, frontier molecular orbital (HOMO and LUMO) energy, and molecular orbitals. Also, since in the default mode, the calculations were done in the gas phase, to simulate a more realistic environment, the calculations were conducted in the presence of three distinct solvents, utilizing similar computational methods and basis sets. Further information about these investigations will be discussed in the following sections. For a better understanding, it is necessary to analyze the reaction mechanism, which showed in Scheme 1. Then, with the help of calculations, the energy of all components was analyzed to check the possibility of the reaction occurrence. Since the reaction we studied has several steps, in order to facilitate the work, all interactions that may occur in each step are investigated thoroughly.

At the beginning of the reaction, the raw material R1 becomes a radical anion by taking an electron from an electrode in the electrochemical cell. The probability of receiving this electron by one of the two double-bonded carbons is higher than the other atoms of the molecule. The π bond receives the electron in the electrochemical cell and turns into β-nitrostyrene radical anion. The radical anion is very active and has a great tendency to react. As a result, after the production of β-nitrostyrene radical-anion, three paths (A, B, and C) and five routes (A1, A2, B, C1 and C2) were designed for this process.

In path A which is depicted in Scheme 2, the β-Nitrostyrene radical anion takes another electron, which leads to the coupling of the single electron of the α carbon. The presence of the nitro electron-withdrawing group causes the relative stability of the negative charge in the β carbon, but the newly produced negative charge in the α carbon is very unstable. At this step, the α carbon electron pair attacks a positive hydrogen that has an empty orbital and forms a bond. This positive hydrogen is probably provided by adding acid to the electrochemical cell.

The product in this step is the first intermediate that we named it I1. After that, intermediate I1 attacks the benzaldehyde's (R2) carbonyl group from β carbon, which has a negative charge, and leads to the breaking of its double bond, and finally the negative charge is transferred to oxygen. after I1 attacks R2 (benzaldehyde), the resulting specie passes through TSI1-I2 transition state and produces intermediate I2. The resulting intermediate I2 leads to the production of an epoxide ring by performing an intramolecular S_N2 reaction and after passing through the TSI2-P1 transition state. In other words, the negatively-charged oxygen attacks the β carbon of I2 by reducing the angle, and causes the C_β-NO_2 bond to break and throw out the nitro group, and as a result, the ring formation reaction and the production of the three-membered ring called epoxy is performed. The requirement for such a reaction is to rotate around the joint bond between β-Nitrostyrene and benzaldehyde so that the NO_2 group is in an anti-state with respect to negative oxygen.

Another possible reaction for intermediate I2 resulting from route A2 is the capture of a proton from H_3O^+ that exists in the electrochemical cell (which may be produced from acid added to the analyte and

absorption of proton by the H_2O molecule) by negative charge oxygen and the formation of a hydroxy group, which results in product P2.

In the next pathway, which is named path B and depicted in Scheme 3, the β-Nitrostyrene radical anion, which has negative charge electron pairs gets protonated in β carbon, and produces the intermediate I3, which is a radical compound itself. After that, I3 reacts radically with benzaldehyde. The double bond of the carbonyl group in benzaldehyde breaks, one of the electrons involved in the bond forms a new bond with the radical on the α carbon of R1-ra. The other single electron of the broken double bond transfers on the carbonyl oxygen. This process passes the TSI3-I4 transition state and produces the intermediate I4. Additionally, hydrogen with a positive charge can be converted into radical hydrogen by taking an electron. Therefore, the best option for radical oxygen in I4 with lack of electron, is to attach to radical hydrogen and produces P3.

R1-ra can also undergo a coupling reaction with itself (dimerization), which is normally performed in the electrochemical reaction of nitrostyrene in the absence of another reactant. Via this route, which named C1 and shown in Scheme 4, the β-nitrostyrene radical anion reacts with its neutral specie, R1. In this way, the radical on α carbon of this compound creates a new bond with one of the electrons resulting from breaking the β-nitrostyrene double bond, and after passing through the transition state of TSR1-I6, it produces a new radical anion, which is called intermediate I6.

I6 intermediate has a negative charge and a single-electron on two β carbons of two coupled β-nitrostyrenes. Initially, the carbon radical receives a radical hydrogen from the solution to achieve sp^3 hybridization, as shown in scheme 4. The other carbon in I6 has negative charge pair electrons, so it similarly receives a hydrogen from the H_3O^+ molecule and turns into the P4 product.

The next route (C2, Scheme 4, down) is similar to the previous route and leads to the same product. The difference between these paths is in one of the raw materials. If the amount of produced radical anion is high and these molecules are stable in the environment, the probability of an anion radical reacting with the same species increases and it dimerize via path C2. The single electrons of these two molecules pair together and form a new bond, which is the coupling of two R1-ra. This process passes through the TSR1-I5 transition state and leads to the production of intermediate I5. The produced intermediate has a negative charge on each of the β carbons of its constituent molecules. According to the mechanism of the C2 route, taking two protons from H_3O^+ by negative charge paired electrons in two distinct steps, leads to the production of P4 product.

3.2. Optimized structures and molecular parameters

For the brief mentioning of the structures, abbreviations were used in this study. Starting materials were defined as R (reactant), intermediates with I, transition states with TS (Transition State) and products with P. There are three starting materials R1, R2 and R1-ra, six intermediates I1, I2, I3, I4, I5 and I6, five transition states TSR1-I1, TSI1-P1, TSI3-I4, TSR1-I6, TSR1-I5, and four products P1, P2 P3 and P4. The optimized structures of all of these compounds are displayed in Fig. 1. Moreover, the important

structural parameters of the bonds and angles involved in the reaction (which includes α and β carbon and NO_2) were investigated in all species, which are listed in Table 1. By examining the bond length of α and β carbons, it was found that the maximum value belongs to P4 and the least value belongs to R1. The reason for the short length of this bond in β-nitrostyrene is due to sp^2 hybridization and creating a double bond between these two carbons. As we know, the higher the percentage of **s** orbital in hybridization, the closer it is to the nucleus, and as a result, the bond length becomes shorter. Another reason that can be attributed to this bond length is the resonance between the double bond and the benzene ring.

The reason for the long length of the C_α-C_β bond can be attributed to the change of hybridization from sp^2 to sp^3 and the decrease in the percentage of **s**. Also, if we pay attention to the structure of this molecule given in Fig. 1, we will see that nitro groups on both sides of the molecule are placed in front of the benzene ring, which creates a repulsion between these two parts, and to reduce this repulsion, the distance between these two is increased, which leads to an increase in the length of bond between α and β carbon to some extent.

If we consider β-nitrostyrene, which is the starting material of the reaction, as a criterion and compare the rest of the parameters with respect to the values obtained from this specie, we find that the length of the C_α-H_α bond is shortened by giving electrons to β-nitrostyrene. In the next step, by giving it a proton, it has become shorter, from 1.085 to 1.083 Å, and finally it has reached 1.081 Å which is the lowest value of the desired bond length. The justification that can be given for this is that vinyl radical has a **p/sp** orbital and are very similar to carbocations in terms of electron deficiency, so they choose a hybridization where the percentage of the **s** orbital has reached zero. Therefore, a single electron is placed in an unhybridized **p** orbital. On the other hand, the bonds have **sp** hybridization, which has a high percentage of **s**, so this makes the length of the C_α-H_α bond stronger and shorter.

These values indicate that the C_α-H_α bond length in the transition state between I3-I4 has the same length as the raw material. Intermediate I3 is formed from the protonation of the β-nitrostyrene radical anion, and because it is a state between the conversion of I3 to I4, by approaching benzaldehyde to intermediate I3 and sharing one electron from both reactants, the single electron moves away from I3 and approaches the neutral state of β-nitrostyrene, so the C_α-H_α bond length is not different from R1. The greatest change in the bond length of α carbon and the hydrogen attached to it is observed in I1 and TSI1-I2. Intermediate I1 is formed by receiving an electron and a proton by the β-nitrostyrene anion radical. This electron is paired with a single radical electron and this produced pair of electrons forms a bond with a proton, and finally the α carbon will have **sp^3** hybridization. Because the percentage of **s** decreases with respect to R1, as a result, the hydrogen moves away from the nucleus and the bond length becomes longer. Regarding the transition state of TSI1-I2, it should be said that because the β carbon is involved in this reaction, this interaction does not have much effect on the length of the C_α-H_α bond.

According to Table 1, the bond length of C_β-H_β in I1 decreased compared toβ-nitrostyrene and P2 showed the most increase in this bond length. As we discussed in the previous section, in radical species, the hydrogen attached to the carbon next to it has a longer length than normal. In this case, because the radical is neutralized, the mentioned bond length has reduced. The N-O bond length in β-nitrostyrene has a value of 1.212Å, according to which TSI2-P1 with a value of 1.190Å has the lowest bond length among all species. The reason why the length of nitrogen-oxygen bond in these molecules is shorter than the starting material, can be related to the resonance of this group when the NO_2 group is separating from the molecule.

Looking at the data of the H_α-C_α-C_β angle we find that the lowest and highest angles correspond to P4 and I3, respectively. In the three-dimensional structure of the P4, the α carbon has **sp^3** hybridization. Carbon with sp3 hybridization usually has an angle of 109.5 degrees. If we compare the P4 product with a simple molecule like methane that has **sp^3** hybridization, we realize that it has an angle of less than 109.5 degrees. The reason for this can be due to the replacement of bulkier groups than simple hydrogen around the carbon. In other words, around the α carbon in P4, a β-nitrostyrene molecule, a benzene ring and a nitro group attached to CH_2, are substituted. Also, the mutual placement of two benzene rings causes steric hindrance and as a result more bending of the mentioned bond, which leads to less angle of this bond.

Compound I3 is a radical with **sp^2** α carbon and **sp^3** β carbon. A simple compound with **sp^2** hybridization has an angle of 120 degrees, which is almost acceptable by having a value of 118.7˚and justifying that one of the groups attached to this carbon is the bulky ring of benzene. However, in the H_α-C_α-C_β angle, β carbon plays an important role because the data in Table 1 show that the β carbon in compound I3 has an angle of 117.2˚, which is much higher than 109.5 degrees. On the other hand, after the radical hydrogenation of the β-nitrostyrene radical anion, this compound transforms from flat state and increases compared to the angle of 116.4˚ in R1-ra. The reason for this can be due to the change of β carbon hybridization from **sp^2** to **sp^3** during the hydrogenation reaction.

In the next case, we will analyze the H_β-C_β-C_α angle. In this case, the highest angle is 128.4˚, belongs to R1. Since the bond between carbon α and β is double, this compound is very similar to the double bond in the ethylene compound. The H_β-C_β-C_α angle in the ethene compound is 120.2˚, which differs by about 8 degrees from the same angle in β-nitrostyrene. This difference is related to the groups connected to the two desired carbons. This means that the steric hindrance created by the benzene and nitro group has caused this angle change.

The lowest value for H_β-C_β-C_α angle with a value of 110.8˚ corresponds to P4. If we pay attention to the intermediate I6 that was before P4, we will notice that the angle has changed from 121.5˚ in this specie to 110.8˚ in the desired product. Therefore, by taking one electron and two hydrogens in separate steps, I6 has changed from a radical anion to a neutral specie, which has been associated with a decrease in angle. Intermediate I6 initially took an electron to convert radical carbon with **p/sp^2** hybridization to

sp^3/sp^3 hybridization. Because in carbanions, the higher the percentage of **s**, the closer the orbital is to the nucleus, and as a result, the more stable the electron is. Now, by taking two hydrogens each by a carbanion, two neutral **sp^3** carbons are produced, that with an angle of 110.8˚ is very close to the angle of methane which is 109.5˚. The difference between these two values is due to the replacement of the bulky group of nitro with hydrogen.

The next studied angles are the angle between nitrogen and β carbon and hydrogen attached to it, as well as the O-N-O angle. Because the intermediate I2 reaches the product P1 with the loss of NO2, this product does not have a nitro group and no data is reported for it.

The highest value for is H_β-C_β-N angle with a value of 115.7˚ corresponding to I1 and the lowest with a value of 92.7˚ corresponding to TSI2-P1. I1 is a carbanion and has a negative charge. According to Fig. 1, the bond between β carbon and nitrogen is close to the double bond state and therefore has **sp^2** hybridization. Additionally, since the nitro group has become flat, the alignment of oxygen and α carbon causes steric hindrance and as a result leads to an increase in the H_β-C_β-N angle.

As shown in the TSI2-P1 image in Fig. 1, oxygen attacked the β carbon by performing the S_N2 reaction and caused the NO_2 to move away. Due to the location of the two benzene rings, there is a steric hindrance between these two, and because the nitro group is placed between these two rings, it is inclined to the outside of the range between the two rings to reduce this tension. Examining the three-dimensional structure determined that the NO_2 group changed the angle in such a way that the H_β-C_β-N angle became smaller.

In the last case, we will discuss about the O-N-O angle. This angle in a free NO_2 group is 134˚. The lowest value of this angle is related to the intermediate I5 at the rate of 118.4˚, which is less than 134˚. The reason for this observation is due to the presence of electrons on the carbon attached to the nitro group, which has the ability to resonate with this group. Both free and negative charged NO_2 are bended, but free NO_2 has a single electron on nitrogen, while negatively charged NO_2 has a pair of non-bonded electrons that repel the bonded electrons and cause the bonds to approach, ultimately causes reducing of the angle O-N-O. The highest value of this angle with 130.2 ˚ belongs to the TSI2-P1transition state. According to the reason described for the reduction of the Hβ-Cβ-N angle, in order to reduce the steric hindrance effect of the two benzene rings on the nitro group, this group, in addition to tending towards the side with less tension, it increases the ONO angle, which has caused an incremental change of 6.5 degrees compared to the intermediate I2.

3.3 The energy profiles of the reaction paths in the gas phase

As we mentioned before, all these molecules were optimized with the M06-2X/Def2TZVP level of theory, and each of these optimized structures was examined to determine the value of zero-point energy (ZPE), enthalpy (H), total electronic energy (E) and their Gibbs free energy (G). Considering that each calculation

method has its own correction coefficient, the correction coefficient value of our studied method was 0.97. Therefore, all of these data were corrected ad used for the relative energies.

In calculating the relative energies, we assume the energy of the starting materials to be zero and calculate the energy of other species versus it. This energy is a measure of whether a reaction is feasible or not, which was calculated step by step for each general route. Gibbs free energy can also be obtained for transition states, that is indicated by the symbol $\Delta G^{\#}$. Since the general reaction was divided into three paths (A, B, and C), the energy of each of them will be explained separately in the next paragraphs.

The gas phase relative Gibbs free energies of all paths, including the path A (which graphically presented in Scheme 2), are presented in Table 2 and the graphical presentation of these reaction pathways were depicted in Fig. 2. Via path A, the radical anion with a radical hydrogen produces intermediate I1, with a relative energy equal to -52.76 kcal/mol, which indicates that this reaction can be carried out thermodynamically. The amounts of relative energies for the of the next transition state TSI1-I2 and intermediate are is respectively − 48.22 and − 49.85 kcal/mol, which means the barrier height ($\Delta G^{\#}$) of this step (versus I1) is 4.54 kcal/mol and ΔG for I1 to I2 conversion is + 2.91 kcal/mol. In the continuation, intermediate I2 converts to P1 via TSI2-P1 and next also convert to P2. Noticeably, because of the barrier energy of proton transfer steps are normally small, any transition states have not been considered for these steps. The relative G of TSI2-P1 and P1 are 21.29 and − 49.97 kcal/mol, respectively, which indicates the non-spontaneous formation of the transition state and then the thermodynamic favorability of product formation. In other words, if the energy required to pass through the transition state energy barrier is provided, the formation of the product can be performed without a problem. It is known that by small heating of the solution, the barrier of about 21 kcal/mol could be passed. Interestingly, the conversion of I2 to P2 (by only protonation) has ΔG equal to -233.40 kcal/mol (relative to of reactants). It seems that in the presence of enough proton source (the high acidity of the reaction media), P2 is more favorable than P1 in high extent an if we need to produce P1, we should control the pH of the solution.

In path B, the energy increases to 2.71 kcal/mol by converting I1-ra to I3, which show that the radical anion I1-ra is more stable than its radical form, I3. This number shows that this step is not thermodynamically favorable. In the next step (conversion of I3 to I4 via TSI3-I4), the TS has relative G equal to 29.81 kcal/mol and the product has relative G equal to 23.35 kcal/mol. These values show that by both thermodynamic and kinetic values, this path is less favorable than path A. At the last step of this path (producing P3 from I4), the relative G of the product is -74.18 kcal/mol. The formation of the product in this path is very exothermic but the previous intermediate and transition state have the high energies, which make this path unfavorable.

In path C (dimerization), the coupling of R1-ra with R1 happened along with the formation of the transition state of TSR1-I6, that its relative Gibbs energy is 21.59 kcal/mol. The production of I6 via this step is also endothermic with an amount of 18.20 kcal/mol, which is not so high. After that, the formation of product P4 is done with an energy of -82.13, which is highly exothermic and favorable, more

than P1 and P3, but less than P2 (this is pH-independent product). In a parallel way, the coupling of two radical anions leads to the production of I5 via TSR1-I5 with a very high barrier, equal to 77.59 kcal/mol. Moreover, the production of I5, needs to of 53.04 kcal/mol energy that make this route impossible.

In conclusion, three paths (A, B, and C), 5 routes (A1, A2, B, C1, and C2) and 4 products (P1 to P4, routes C1 and C2 produce similar product) have been investigated in this part. The first two paths involve with the reaction of nitrostyrene radical anion with benzaldehyde. Comparing these two paths, path A is preferred thermodynamically and kinetically (versus path B and producing P3). Comparing the two routs of path A shows that route A2 and product P2 is more favorable than route A1 and product P1; but producing P2 needs to a high concentration of proton source. This means that by increasing the pH, product P1 is preferred and in small pH values, P2 is preferred.

The next path (C), includes the dimerization, which is different form the first two paths. Both routes of this path lead to the similar product (P4). However, the barrier energy of route C1 is less than C2 and this route is preferred. This path could be performed in the absence or small concentration of benzaldehyde. The overall barriers of these five routes (the energy in parentheses refers to the relative G versus reactants in kcal/mol) are in this order: A2 (-48.22) < A1 (21.29) < C1 (21.59) < B (29.81) < C2 (77.59). The ΔG for the formation of four products (the energy in parentheses refers to the relative G versus reactants in kcal/mol) are in this order: P2 (-233.40) < P4 (-82.13) < P3 (-74.18) < P1 (-46.97). Therefore, in the extra amount of both benzaldehyde and proton, P2 is the major product, in the extra amount of benzaldehyde and minimum amount of proton, P1 is preferred, and in the small amount of benzaldehyde and proton, P4 is preferred (only via C1 route). The routes B and C2 have the highest barriers and are unfavorable. So that, producing P3 is also unfavorable.

3.4 The solvent effects

Since the studied reaction is actually and practically done in the liquid phase, in addition to the previous calculations that were done in the gas phase by default, all those calculations were also done for three different solvents. For this purpose, three water, methanol and dimethylformamide were selected as three common protic and aprotic solvent. These solvents are used in the electrochemical reactions, more than the other solvents. In addition to being cheap and safe, the reason for choosing water was its high solubility, adequate polarity, and the ability to form hydrogen bonds. Dimethylformamide is an aprotic solvent, with a polarity lower than water, but suitable for the electrochemical reactions, with a high dielectric constant. Also, methanol, an active protic solvent, with a high polarity and high solubility, which has the ability to increase reaction yield.

After the optimization of all structures, the changes of Gibbs free energy and relative energy for each part of the reaction for each solvent were extracted, which will be investigated further in following sections. The relative energies (versus the reactants) of all species in three solvents, comparing with the gas phase data, and the graphical presentation of these data were shown in Table 3 and Fig. 3.

Table 1. Important structural parameters involved in the reaction (bond angles are reported in degrees)

molecule	C_α-C_β (Å)	C_α-H_α (Å)	C_β-H_β (Å)	Avg. N-O (Å)	H_α-C_α-C_β	H_β-C_β-C_α	H_β-C_β-N	O-N-O
R1	1.326	1.085	1.077	1.212	116.7	128.4	111.6	125.1
R1-ra	1.377	1.083	1.078	1.258	116.4	124.9	112.4	121.7
I1	1.490	1.095	1.076	1.272	107.9	123.6	115.7	119.6
I2	1.522	1.091	1.088	1.217	105.5	113.8	104.8	123.7
I3	1.483	1.081	1.087	1.207	117.2	113.5	105.2	125.9
I4	1.523	1.091	1.088	1.207	107.8	112.6	105.6	125.8
I5	1.504	1.092	1.078	1.281	105.8	120.1	113.5	118.4
I6	1.461	1.090	1.078	1.248	106.1	121.5	112	121.2
P1	1.508	1.092	1.089	_	108.7	115.9	_	_
P2	1.518	1.090	1.090	1.207	107.7	111.8	103.6	125.4
P3	1.522	1.092	1.088	1.208	107.9	112.4	105.6	125.6
P4	1.535	1.092	1.087	1.210	103.4	110.8	105.5	125
TSI1-I2	1.502	1.095	1.082	1.238	110.5	119.2	110.7	122
TSI3-I4	1.505	1.085	1.087	1.207	113.1	112.8	105.4	125.9
TSI2-P1	1.511	1.091	1.083	1.190	108.3	118.6	93.7	130.2
TSR1-I6	1.430	1.088	1.080	1.261	107.8	119.9	111.4	121.4
TSR1-I5	1.434	1.086	1.082	1.283	110	118.8	111.6	119.6

Table 2. Relative Gibbs free energy values (in kcal/mol) for all paths					
Path A		Path B		Path C	
R1-ra	0.00	R1-ra	0.00	R1-ra	0.00
I1	-52.76	I3	2.71	TSR1-I6	21.59
TSI1-I2	-48.22	TSI3-I4	29.81	I6	18.20
I2	-49.85	I4	23.35	TSR1-I5	77.59
TSI2-P1	21.29	P3	-74.18	I5	53.04
P1	-46.97			P4	-82.13
P2	-233.40				

Table 3. Relative Gibbs free energy values (kcal/mol) for proposed all paths in three solvents in comparison with the gas phase values

Path A	ΔG_{re} (gas)	ΔG_{re} (DMF)	ΔG_{re} (methanol)	ΔG_{re} (water)
R1-ra	0.00	0.00	0.00	0.00
I1	-52.76	-57.85	-57.82	-57.94
TSI1-I2	-48.22	-42.85	-42.86	-42.80
I2	-49.85	-45.15	-45.15	-45.14
TSI2-P1	21.29	95.60	95.37	96.47
P1	-46.97	-60.23	-60.21	-60.31
P2	-233.40	-112.75	-113.24	-110.93
Path B				
I3	2.71	-37.09	-37.57	-35.31
TSI3-I4	29.81	-8.69	-9.17	-6.90
I4	23.35	-14.95	-15.44	-13.16
P3	-74.18	-112.53	-113.01	-110.73
Path C				
TSR1-I6	21.59	34.10	34.03	34.35
I6	18.20	31.02	30.95	31.28
P4	-82.13	-118.91	-119.40	-117.07
TSR1-I5	77.59	29.21	29.38	28.57
I5	53.04	-0.82	-0.62	-1.56
P4	-82.13	-118.91	-119.40	-117.07

Table 4. Energy of HOMO/LUMO orbitals(eV), energy gap(eV), hardness(eV), softness(eV), chemical potential(eV) and electrophilicity index (1/eV) for all species							
	HOMO	LUMO	E_g	η	S	μ	ω
R1	-0.314	-0.068	-0.245	0.123	8.149	-0.191	2.24E-03
R2	-0.325	-0.036	-0.289	0.144	6.925	-0.180	2.35E-03
R1-ra	-0.031	0.143	-0.174	0.087	11.491	0.056	1.34E-04
I1	-0.005	0.124	-0.129	0.064	15.550	0.059	1.13E-04
I2	-0.111	0.120	-0.232	0.116	8.630	0.004	1.14E-06
I3	-0.251	-0.017	-0.233	0.117	8.569	-0.134	1.05E-03
I4	-0.308	-0.021	-0.288	0.144	6.951	-0.164	1.95E-03
I5	0.015	0.233	-0.218	0.109	9.155	0.124	8.37E-04
I6	-0.090	0.083	-0.173	0.087	11.556	-0.004	6.50E-07
P1	-0.295	0.014	-0.309	0.155	6.471	-0.141	1.53E-03
P2	-0.301	-0.018	-0.283	0.141	7.073	-0.160	1.81E-03
P3	-0.308	-0.018	-0.290	0.145	6.889	-0.163	1.92E-03
P4	-0.311	-0.032	-0.279	0.140	7.163	-0.172	2.06E-03
TSI1-I2	-0.111	0.123	-0.234	0.117	8.546	0.006	1.89E-06
TSI3-I4	-0.299	-0.019	-0.280	0.140	7.138	-0.159	1.77E-03
TSI2-P1	-0.115	0.084	-0.199	0.099	10.071	-0.015	1.17E-05
TSR1-I6	0.049	0.190	-0.141	0.071	14.178	0.120	5.07E-04
TSR1-I5	-0.281	-0.026	-0.255	0.128	7.843	-0.153	1.49E-03

Except for some structure, mostly the solvent data are similar to the gas phase data. By considering the average values, methanol and then DMF (with small amount difference) showed the most stabilizing effect (reducing the energies of the intermediates, products and transition states versus the reactants) and water showed the least stabilizing effect. This order could be related to the dielectric constant of the solvent. Therefore, by decreasing the dielectric constant of the solvent, its stabilizing effect and facilitating the reaction is increased averagely.

After that, the production of intermediate I1 from the binding of radical hydrogen to the β-nitrostyrene radical anion has a value of -52.76 kcal/mol in the gas phase, -57.85 for dimethylformamide, -57.82 for methanol and − 57.94 for water. All these numbers are negative and thermodynamically favorable. Among these four states, the reaction in water solvent is slightly more favorable because it is more negative. The next step, the process of converting I1 to I2, has a transition state TSI1-I2, that its energy

compared to I1 is -48.22 kcal/mol in the gas phase, -42.85 in the solvent dimethylformamide, -42.86 in methanol and − 42.80 in water. In the mentioned three solvents, this step is favorable, but in the methanol, it is a little more favorable than other solvents. After the formation of TSI1-I2, the relative energy of formed I2 intermediate is -49.85 in the gas phase, -45.15 in dimethylformamide and methanol, and − 45.14 kcal/mol in water; Therefore, this reaction is carried out more favorable in the gas phase than in the solvent. The next reaction that leads to the production of product P1 from I2, in the gas phase, dimethylformamide, methanol and water have the amounts of -46.97, -60.23, -60.21 and − 60.31 kcal/mol, respectively and the TSI2-P1 transition state, which is produced in the meantime, in the gas phase, dimethylformamide, Methanol and water have values of 21.29, 95.60, 95.37 and 96.47 kcal/mol, respectively. The formation of the transition state is generally undesirable but more desirable in the gas phase than in the solvent phase. Conversely, the production of P1 in the A1 pathway is more desirable in the solvent phase than in the gas phase. Also, among the three studied solvents, water is slightly more suitable for P1 production. Unlike path A1, the relative energy of the P2 (via route A2) are − 233.40 kcal/mol in the gas phase and is much more favorable than the same reaction in dimethylformamide with an amount of -112.75 kcal/mol, in methanol with − 113.24 kcal/mol and in water solvent with − 110.93 kcal/mol. Comparison of the difference of this number in the three solvents shows that this step is more favorable in methanol solvent than the same reaction in the other two solvents.

In route B, the conversion of the β-nitrostyrene radical anion to I3 occurs first. The related Gibbs free energy change related to this step in the gas phase is 2.71 kcal/mol and in the three solvents dimethylformamide, methanol and water are − 37.09, -37.57 and − 35.31 kcal/mol, respectively. As it is clear, this reaction is unfavorable in the gas phase and highly favorable in all the three solvents (mostly in the methanol and then in DMF). The energy related to the formation of the transition state suddenly declines from 29.81 kcal/mol (in the gas phase) to -8.69, -9.17 and − 6.90 kcal/mol in dimethylformamide, methanol and water, respectively. After that, the formation of I4 takes place, that the relative energies calculated in the gas phase and all three solvents, dimethylformamide, methanol and water, with the amounts of -23.35, -14.95, -15.44 and − 13.16 kcal/mol indicates the higher favorability of this reaction in the solvent phase. The energy values related to the next step which is the conversion of I4 to P3, in the gas phase is -74.18 kcal/mol and in the three mentioned solvents are − 112.53, -113.01 and − 110.73 kcal/mol, respectively; Therefore, the above data show the greater favorability of all parts of this path in the solvent phase compared to the gas phase and in methanol among the three solvents.

In route C1 of path C, β-nitrostyrene radical anion reacts with the neutral β-nitrostyrene molecule through TSR1-I6, that has a relative energy of 21.59 in the gas phase and 34.10, 34.03 and 34.35 in dimethylformamide, methanol and water respectively. Then, the production of intermediate I6 has an energy value of 18.20 kcal/mol in the gas phase, 31.02 in the solvent dimethylformamide, 30.95 in methanol and 31.28 in water. These two steps are thermodynamically unfavorable due to their positive energies, but they are relatively more favorable in the gas phase than the three solvents so they require less activation energy compared to the other three states. Finally, the relative energy for the third step, in the gas phase, dimethylformamide, methanol and water are − 82.13, -118.91, -119.40 and − 117.07

kcal/mol, respectively. In addition to confirming favorability of this product, it shows the favorability of this reaction in three solvents is higher than the gas phase.

In route C2 of path C, the energy of transition state TSR1-I5 is 77.59, 29.21, 29.38 and 28.57 kcal/mol in the gas phase, dimethylformamide, methanol and water. After that, the production of intermediate I5, occur with relative energy at the rate of 53.04 kcal/mol in the gas phase and in three solvents of dimethylformamide, methanol and water with the amounts of -0.82, -0.62 and − 1.56 kcal/mol. These values show that this reaction is thermodynamically favorable in all three solvents, and the energy of this reaction in water solvent is more negative than other solvents.

By thew brief reviewing thermodynamic data (the relative energies of the products versus the reactants), P1 is stabilize in all solvents by about 13 kcal/mol and very small differences are observed for different solvents. P2 is highly destabilize, by about a20 kcal/mol in the solvent; but it still is highly favorable and the relative energies of P2 in DMF, methanol and water are − 112.75, -113.24, and − 110.93 kcal/mol, respectively. However, both P3 and P4 are highly stabilize (about 30–40 kcal/mol) in the solvent versus the gas phase. In all of these products, the stabilizing effect are in this order: methanol > DMF > water.

Kinetic values showed the reverse values. By reviewing the relative energies of the five transition states, only the TSI3-I4 (transition state of the route B) is stabilized and the other transition states are destabilized in the solvents. The average destabilizing effect for TSI1-I2 is ~ 6 kcal/mol, for TSI2-p1 is ~ 74 kcal/mol, for TSR1-I6 is ~ 13 kcal/mol, and for TSR1-I5 is ~ 48 kcal/mol, while TSI3-I4 stabilize in about 38 kcal/mol in the solvents.

In conclusion, despite the gas phase data, path B and product P3 are a favorable path and product. Thermodynamically, the average relative G in three solvents for P3 is -112.09 kcal/mol, for P2 is -112.1, for P4 is -118.46, and for P1 is -60.25. Kinetically, the average relative G in three solvents for the transition states of P3 is -8.25 kcal/mol, P2 is -42.84, P4 is 34.16 via route C1 and 29.05 via route C2, and P1 is 95.81. Therefore, because of the high barriers, products P1 and P4 are less favorable. In the excess concentration of proton, P2 is the most favorable product by both kinetic and thermodynamic data and the for P low concentration of proton, P3 is the most favorable product. It should be mentioned that in the absence of benzaldehyde, producing P4 is possible via C2 (the route with the smaller barrier) by warming to overcome the barrier.

3.5. Population analysis

In order to wealth our information about the chemical and physical properties of studied species, molecular orbitals, including the Highest Occupied Molecular Orbital (HOMO) and the Lowest Unoccupied Molecular Orbital (LUMO), shown in Fig. 4, and the energy gap, hardness and softness, chemical potential, and electrophilicity of them were calculated and listed in Table 4.

After achieving molecular orbital of each compound, we can easily determine HOMO and LUMO and their energy. After that the five parameters mentioned before, were calculated using Eq. 1–5 respectively.

$$E_g = E_{HOMO} - E_{LUMO}$$

(1)

$$\eta = \frac{(E_{LUMO} - E_{HOMO})}{2}$$

(2)

$$S = \frac{1}{\eta}$$

(3)

$$\mu = \frac{(E_{LUMO} + E_{HOMO})}{2}$$

(4)

$$\omega = \frac{\mu^2}{2\eta}$$

(5)

These concepts are interconnected and can be used to predict and explain the behavior of molecules in chemical reactions, their stability, and their interactions with other molecules. the HOMO-LUMO gap can help predict the color of a compound, as the energy of the absorbed energy corresponds to the energy difference between these orbitals. Similarly, hardness and softness can predict the outcome of acid-base reactions using the Hard Soft Acid Base (HSAB) principle. Chemical potential and electrophilicity can be used to understand and predict the course of polar reactions.

Considering the shapes of frontier orbitals (Fig. 4) in r1 (neutral nitrostyrene), the small amount of HOMO distribution is placed on α and β carbons, while the high density is placed on these atoms at LUMO orbitals which showed the higher electrophilic properties of these carbons. Next, in r1-ra (radical anion of nitrostyrene), this reactivity is inversed and the high electron density is placed on these atoms in LUMO is observed. Therefore, the nucleophiles could easily attack to theses carbons in r1 while in r1-ra, this carbon should easily attack to benzaldehyde and there is no meaningful difference between α and β carbons related to this reactivity. In addition, benzaldehyde is known as a good electrophile that could be clearly observed in its LUMO orbital. The similar observation is visible for i1 and i3, which make them able to attack to benzaldehyde. Also, the most of electron distribution in the HOMO of i2, i5, and i6 is observed at α and β carbons.

The reactivity parameters (Table 4), showed large increase in the HOMO energy and the obvious decrease in the energy gap of r1-ra versus r1, confirming its higher reactivity, especially as nucleophile. The energy gaps of the product are obviously larger than their relative intermediates and transition state, confirmed their stabilities. The electrophilicity index of r11-ra is also less than r1 and its chemical

potentials are larger. The chemical potentials of the products are also smaller than the other species, in general.

4. Conclusion

In this study, the electrochemical reaction between β-nitrostyrene and benzaldehyde were investigated theoretically, in competition with its dimerization, were investigated. In this line, 3 paths, 5 routes and 4 possible products were included to find the best way in the gas phase and three different solvents. Our findings in the gas phase indicated that the lowest energy barrier corresponds to product P2. Remarkably, P2 also exhibits the lowest energy among all the products considered. Notably, P2 satisfies the criteria for both a favorable kinetic product and a favorable thermodynamic product, suggesting its dual favorability. In the dimethylformamide solvent, the lowest energy barrier pertains to product P3, emphasizing its kinetic favorability. Interestingly, the P4 product resulting from both pathways shares identical energy levels, yet the energy barriers associated with each path differ. Consequently, in dimethylformamide, the thermodynamic product is identified as P4), considering the higher energy barrier of the C1 path relative to C2. Turning our attention to the methanol solvent, we found that P3 remains the kinetic product due to its minimal energy barrier. Analogously to dimethylformamide, the P4 product emerges as the thermodynamic choice in methanol. Lastly, in the water solvent, the lowest energy barrier aligns with product P2, suggesting its kinetic favorability. Additionally, the P4(I5) and P4(I6) products share identical energies, both being the lowest among all products. Consequently, one of these two paths likely leads to the production of a thermodynamic product. Given the higher energy barrier associated with P4, it is identified as the thermodynamic product in water.

Declarations

Author Contribution

D. Shirvani performed the calculations and extracted the dataH. Tavakol designed the study, supervised the work, checked the data and corrected and submitted the manuscriptM. Abedini wrote the manuscript draft

References

1. Melot, B.C. and J.-M. Tarascon, *Design and preparation of materials for advanced electrochemical storage.* Accounts of chemical research, 2013. **46**(5): p. 1226-1238.
2. Marčeková, M., et al., *Denitrative cross-couplings of nitrostyrenes.* Molecules, 2020. **25**(15): p. 3390.
3. Shamsaddinimotlagh, S., et al., *Solvent-Free Synthesis of α-Cyanophosphonates from β-Nitrostyrenes by Using a Deep-Eutectic Solvent Catalyst.* Synlett, 2024.
4. Ranjbari, M. A., Tavakol, H., & Manoukian, M. (2021). Regioselective and solvent-free arylation of β-nitrostyrenes with mono-and dialkyl anilines. Research on Chemical Intermediates, 47, 709-721.

5. Abtahi, B. and H. Tavakol, *Conversion of β-Nitrostyrenes to Naphthofurans via a Cascade Reaction with α-and β-Naphthols.* ChemistrySelect, 2020. **5**(40): p. 12582-12585.
6. Anan, A., et al., *Controlled Synthesis of the Henry Reaction Products: Nitroalcohol Versus Nitrostyrene by a Simple Change of Amino-Groups of Aminofunctionalized Nanoporous Catalysts.* Catalysis letters, 2008. **126**: p. 142-148.
7. Ying, A., et al., *Novel multiple-acidic ionic liquids: catalysts for environmentally friendly benign synthesis of trans-β-nitrostyrenes under solvent-free conditions.* Industrial & Engineering Chemistry Research, 2014. **53**(2): p. 547-552.
8. Grossi, L., P.C. Montevecchi, and S. Strazzari, *The chemistry of peroxynitrite: involvement of an ET process in the radical nitration of unsaturated and aromatic systems.* European Journal of Organic Chemistry, 2001. **2001**(4): p. 741-748.
9. Milhazes, N., et al., *β-Nitrostyrene derivatives as potential antibacterial agents: A structure–property–activity relationship study.* Bioorganic & medicinal chemistry, 2006. **14**(12): p. 4078-4088.
10. Rostami, H. and L. Shiri, *Application of β-Nitrostyrene in Multicomponent Reactions for the Synthesis of Pyrrole Derivatives.* ChemistrySelect, 2020. **5**(36): p. 11197-11220.
11. Tsai, C.-H., et al., *3'-Hydroxy-4'-methoxy-β-methyl-β-nitrostyrene inhibits tumor growth through ROS generation and GSH depletion in lung cancer cells.* Life sciences, 2017. **172**: p. 19-26.
12. Gavin, D.P. and J.C. Stephens, *Organocatalytic enantioselective Michael addition of β-diketones to β-nitrostyrene: The first Michael addition of dipivaloylmethane to an activated olefin.* Arkivoc, 2011. **2011**(9): p. 407-421.
13. Wang, J., et al., *Enantio-and diastereoselective Michael addition reactions of unmodified aldehydes and ketones with nitroolefins catalyzed by a pyrrolidine sulfonamide.* Chemistry–A European Journal, 2006. **12**(16): p. 4321-4332.
14. Wonner, P., et al., *Chalcogen bonding catalysis of a nitro-Michael reaction.* Angewandte Chemie International Edition, 2019. **58**(47): p. 16923-16927.
15. Ríos-Gutiérrez, M., L.R. Domingo, and R. Jasiński, *Understanding the different reactivity of (Z)-and (E)-β-nitrostyrenes in [3+ 2] cycloaddition reactions. An MEDT study.* RSC advances, 2021. **11**(16): p. 9698-9708.
16. Wade, P.A., et al., *Sequential Diels–Alder/[3, 3]-sigmatropic rearrangement reactions of β-nitrostyrene with 3-methyl-1, 3-pentadiene.* Beilstein Journal of Organic Chemistry, 2013. **9**(1): p. 2137-2146.
17. Chen, Z.G., P.F. Zhao, and Y. Wang, *Aminobromination of β-Nitrostyrene Derivatives with N, N-Dibromourethane as the Aminobrominating Reagent*. 2011, Wiley Online Library.
18. Chen, Z.-G., et al., *K3PO4-catalyzed regiospecific aminobromination of β-nitrostyrene derivatives with N-bromoacetamide as aminobrominating agent.* The Journal of Organic Chemistry, 2010. **75**(6): p. 2085-2088.
19. Zhi, S., et al., *The combination of benzamides/NCS as nitrogen/halogen sources for aminohalogenation of β-nitrostyrenes resulting in dichlorinated haloamides.* Science China

Chemistry, 2010. **53**: p. 1946-1952.

20. Milhazes, N., et al., *Identification of synthetic precursors of amphetamine-like drugs using Raman spectroscopy and ab initio calculations: β-Methyl-β-nitrostyrene derivatives.* Analyst, 2004. **129**(11): p. 1106-1117.
21. d'Andrea, L. and J.L. Kristensen, *One-pot Reduction of Nitrostyrenes to Phenethylamines using Sodium Borohydride and Copper (II) chloride.* 2023.
22. Ranjbari, M.A., H. Tavakol, and M. Manoukian, *Regioselective and solvent-free arylation of β-nitrostyrenes with mono-and dialkyl anilines.* Research on Chemical Intermediates, 2021. **47**: p. 709-721.
23. Dalinger, A.I., et al., *Reaction of β-Nitrostyrene with Diethyl Malonate in the Presence of Bispidines: The Unusual Role of the Organocatalyst.* Chemistry, 2024. **6**(3): p. 387-406.
24. Khorshidvand, N., Kassaee, M. Z., & Safaei, S. (2020). Substituent effects on novel diaminovinylidenes by DFT. Research on Chemical Intermediates, 46, 2289-2308.
25. Orupattur, N.V., S.H. Mushrif, and V. Prasad, *Catalytic materials and chemistry development using a synergistic combination of machine learning and ab initio methods.* Computational Materials Science, 2020. **174**: p. 109474.
26. Westermayr, J., et al., *Perspective on integrating machine learning into computational chemistry and materials science.* The Journal of Chemical Physics, 2021. **154**(23).
27. Gayathiri, E., et al., *Computational approaches for modeling and structural design of biological systems: A comprehensive review.* Progress in Biophysics and Molecular Biology, 2023.
28. Schreckenbach, S.A., et al., *Predicting the mass spectra of environmental pollutants using computational chemistry: A case study and critical evaluation.* Journal of the American Society for Mass Spectrometry, 2021. **32**(6): p. 1508-1518.
29. Ahn, S., et al., *Design and optimization of catalysts based on mechanistic insights derived from quantum chemical reaction modeling.* Chemical reviews, 2019. **119**(11): p. 6509-6560.
30. Jiang, H., et al., *Theoretical study on mechanism of cinchona alkaloids catalyzed asymmetric conjugate addition of dimethyl malonate to β-nitrostyrene.* International Journal of Quantum Chemistry, 2014. **114**(10): p. 642-651.
31. Kula, K. and K. Zawadzińska, *Local nucleophile-electrophile interactions in [3+ 2] cycloaddition reactions between benzonitrile N-oxide and selected conjugated nitroalkenes in the light of MEDT computational study.* Current Chemistry Letters, 2021. **10**(1): p. 9-16.
32. Gan, L.-H., J. Zhou, and X. Guo, *The reaction mechanisms of aldehydes and nitrostyrene catalyzed by a chiral silylated pyrrolidine catalyst.* Journal of Theoretical and Computational Chemistry, 2013. **12**(03): p. 1350004.
33. Wang, L., *Computational Study of Catalytic Activity of a HD-Pro-Pro-Glu-NH 2 Derivatives in an Emulsion*. 2021, Clemson University.

34. Sun, S., et al., *From Charge to Spin: An In-Depth Exploration of Electron Transfer in Energy Electrocatalysis.* Advanced Materials, 2024: p. 2312524.
35. Muhammad, H., Hanif, M., Tahiri, I. A., Versiani, M. A., Shah, F., Khaliq, O., ... & Ahmed, S. (2018). Electrochemical behavior of superoxide anion radical towards quinones: a mechanistic approach. Research on Chemical Intermediates, 44, 6387-6400.
36. DeCaluwe, S.C., et al., *On the fundamental and practical aspects of modeling complex electrochemical kinetics and transport.* Journal of The Electrochemical Society, 2018. **165**(13): p. E637.
37. Sbei, N., Titov, A. A., Karthikeyan, S., & Voskressensky, L. G. (2020). Efficient synthesis of imino-1, 3-thiazinan-4-one promoted by acetonitrile electrogenerated base and computational studies with CB1 and 11 βHSD1 molecules. Research on Chemical Intermediates, 46, 5535-5545.
38. Maia, P. J. S., Cruz, J. F., de Freitas, F. A., de Fátima Freire dos Santos, S., & de Souza, E. A. (2019). Photophysical properties of a perylene derivative for use as catalyst in ethanol eletrooxidation. Research on Chemical Intermediates, 45, 5451-5472.
39. Calle-Vallejo, F. and M.T. Koper, *First-principles computational electrochemistry: Achievements and challenges.* Electrochimica Acta, 2012. **84**: p. 3-11.
40. Bollo, S., et al., *Electrochemical study of nitrostilbene derivatives: nitro group as a probe of the push–pull effect.* Journal of Electroanalytical Chemistry, 2000. **492**(1): p. 54-62.
41. Tavakol, H., Ranjbari, M. A., & Jafari-Chermahini, M. T. (2019). Mechanistic details for the reaction of methyl acrylate radical anion: a DFT study. *Reaction Kinetics, Mechanisms and Catalysis*, *128*, 629-643.
42. Ranjbari, M. A., & Tavakol, H. (2018). Theoretical study of the possible mechanisms for the synthesis of dialkyl thiourea from dithiocarbamate. *Heteroatom Chemistry*, *29*(3), e21421.
43. Tavakol, H. (2011). DFT and MP2 study of simple and water-assisted tautomerism in amidrazones. *Structural Chemistry*, *22*(5), 1165-1177.
44. Tavakol, H., & Shafieyoon, P. (2023). The theoretical study of electron-induced trimerization of acrylic acid anion radical in the gas phase. Research on Chemical Intermediates, 49(8), 3645-3658.
45. El-Azhary, A. and H. Suter, *Comparison between optimized geometries and vibrational frequencies calculated by the DFT methods.* The Journal of Physical Chemistry, 1996. **100**(37): p. 15056-15063.
46. Praveen, P.L. and D.P. Ojha, *Role of molecular interactions and end chain length on the photosensitivity of liquid crystalline alkyl cyanobiphenyl dimers–UV absorption-based approach through DFT calculations.* Phase Transitions, 2014. **87**(7): p. 641-655.
47. Saxena, A., M. Agrawal, and A. Gupta, *Vibrational study, molecular properties and first-order molecular hyperpolarizability of Methyl 2-amino 5-bromobenzoate using DFT method.* Optical Materials, 2015. **46**: p. 154-167.
48. Wang, Y., et al., *M06-SX screened-exchange density functional for chemistry and solid-state physics.* Proceedings of the National Academy of Sciences, 2020. **117**(5): p. 2294-2301.

49. Ndagi, U., M.M. Lawal, and M.E. Soliman, *DFT study of the structural and electronic properties of selected organogold (III) compounds with characteristic anticancer activity.* Russian Journal of Physical Chemistry A, 2019. **93**: p. 1543-1558.
50. Frisch, M.J.T., G. W.; Schlegel, H. B.; Scuseria, G. E.; Robb, M. A.; and J.R.S. Cheeseman, G.; Barone, V.; Petersson, G. A.; Nakatsuji, H.; Li, X.; Caricato, M.; Marenich, A. V.; Bloino, J.; Janesko, B. G.; Gomperts, R.; Mennucci, B.; Hratchian, H. P.; Ortiz, J. V.; Izmaylov, A. F.; Sonnenberg, J. L.; Williams-Young, D.; Ding, F.; Lipparini, F.; Egidi, F.; Goings, J.; Peng, B.; Petrone, A.; Henderson, T.; Ranasinghe, D.; Zakrzewski, V. G.; Gao, J.; Rega, N.; Zheng, G.; Liang, W.; Hada, M.; Ehara, M.; Toyota, K.; Fukuda, R.; Hasegawa, J.; Ishida, M.; Nakajima, T.; Honda, Y.; \Kitao, O.; Nakai, H.; Vreven, T.; Throssell, K.; Montgomery, J. A., Jr.; Peralta, J. E.; Ogliaro, F.; Bearpark, M. J.; Heyd, J. J.; Brothers, E. N.; Kudin, K. N.; Staroverov, V. N.; Keith, T. A.; Kobayashi, R.; Normand, J.; Raghavachari, K.; Rendell, A. P.; Burant, J. C.; Iyengar, S. S.; Tomasi, J.; Cossi, M.; Millam, J. M.; Klene, M.; Adamo, C.; Cammi, R.; Ochterski, J. W.; Martin, R. L.; Morokuma, K.; Farkas, O.; Foresman, J. B.; Fox, D. J. , *Gaussian 09, Revision B.01.* 2016.

Schemes

Schemes are available in the Supplementary Files section.

Figures

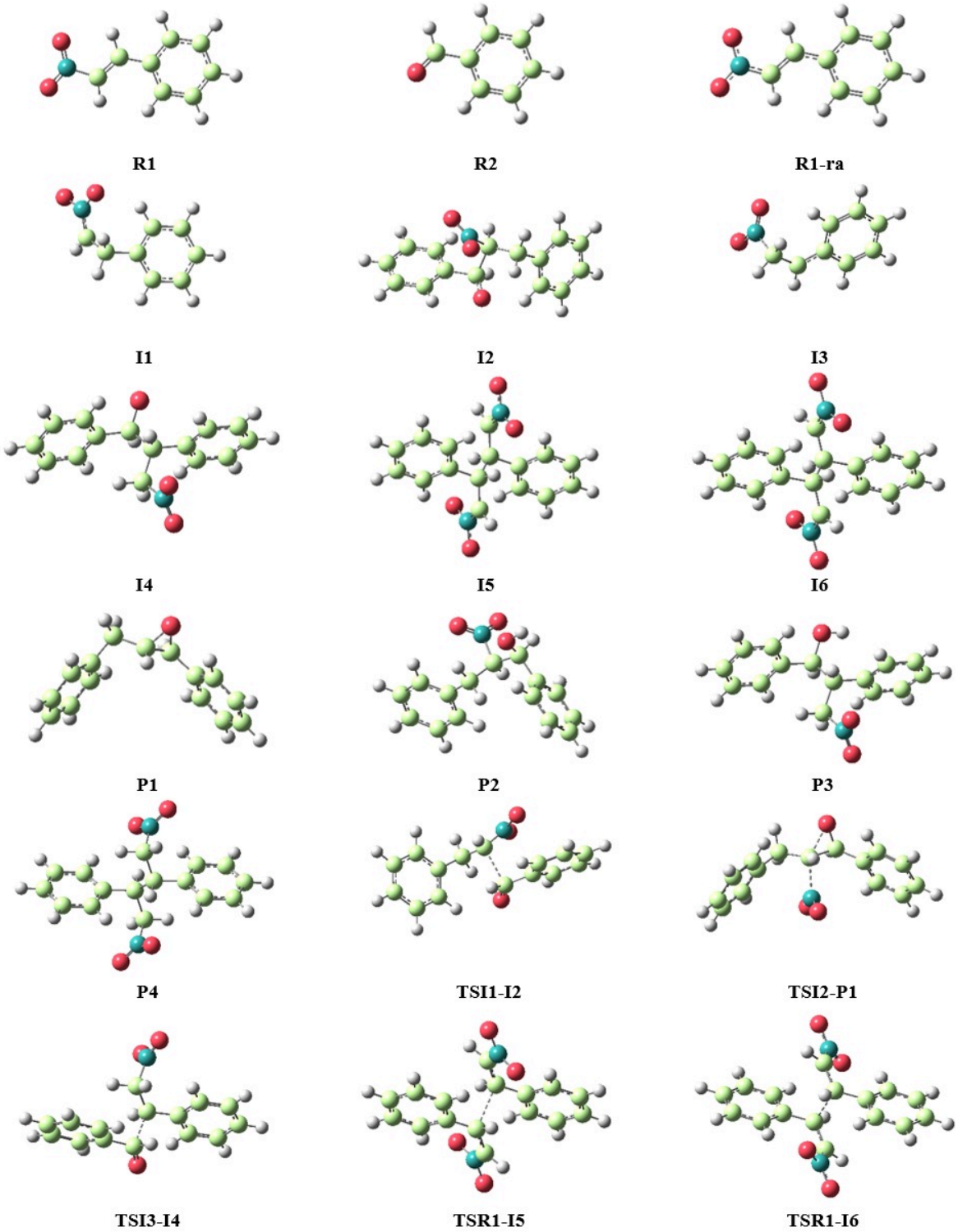

Figure 1

M062x/def2tzvp optimized structures of all reactants, intermediates, transition states and products

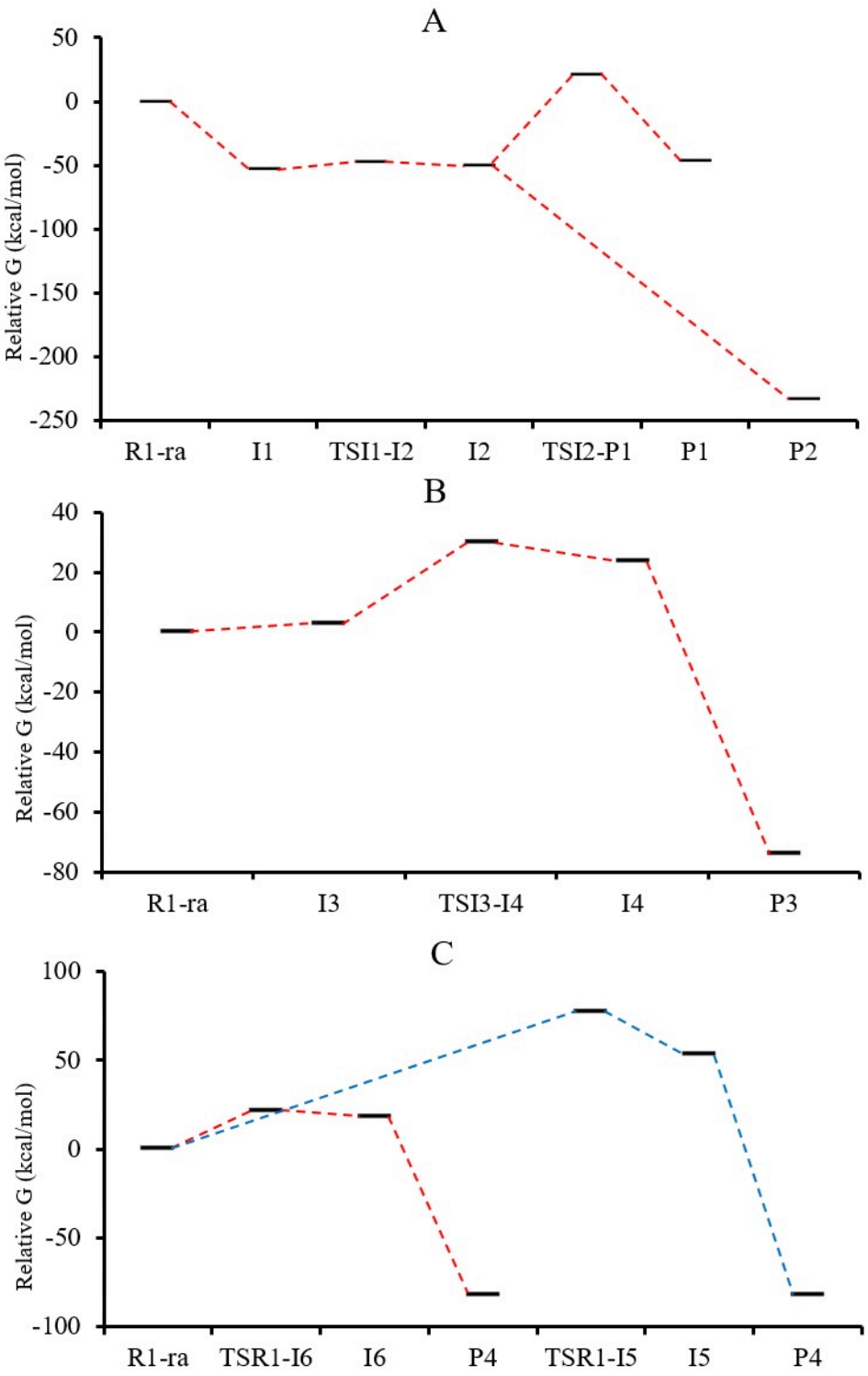

Figure 2

Diagram of relative ΔG values for all paths in the gas phase

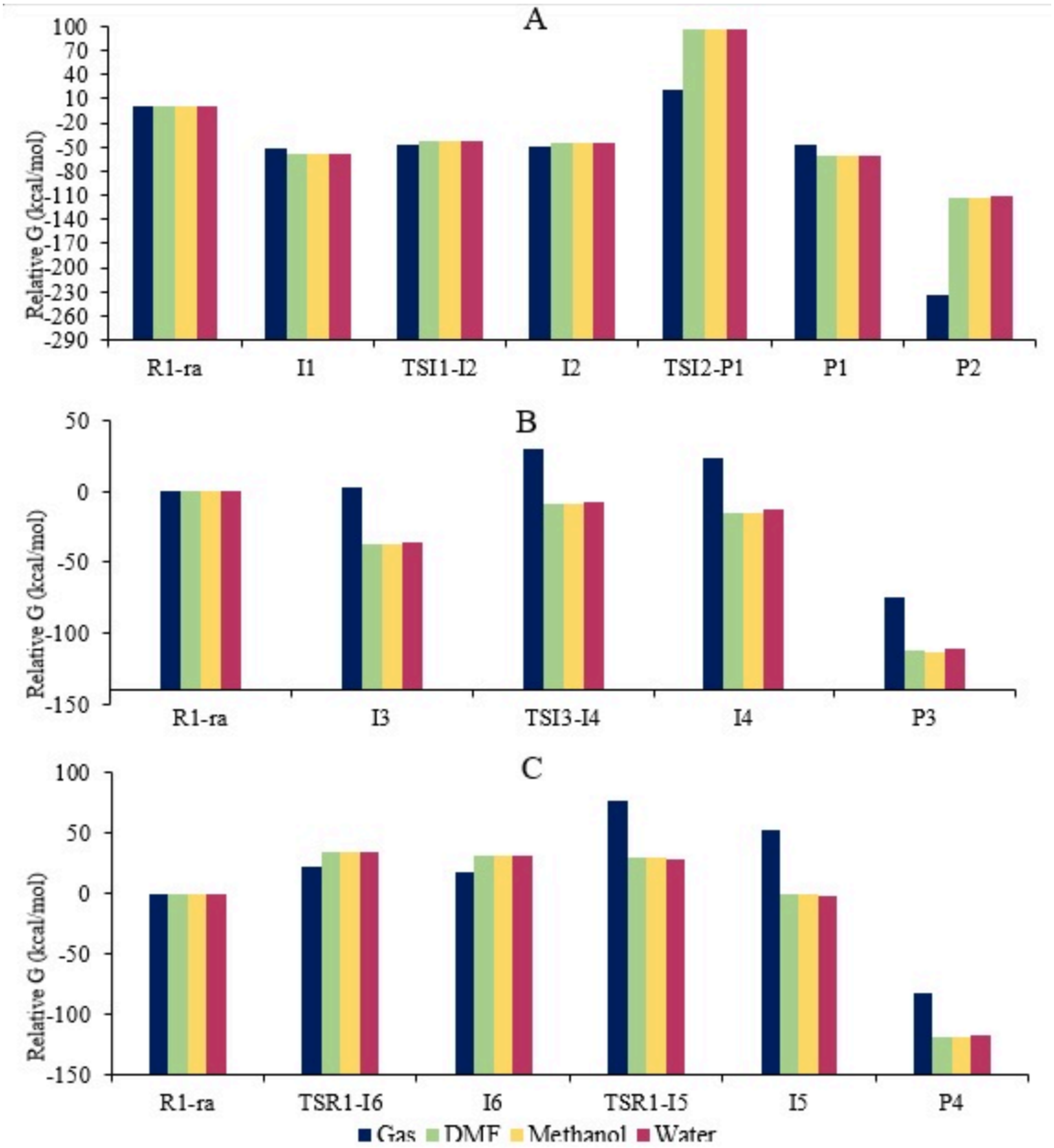

Figure 3

Diagram of relative ΔG values for all paths in three solvents: dimethylformamide, methanol, and water, comparing with the gas phase values

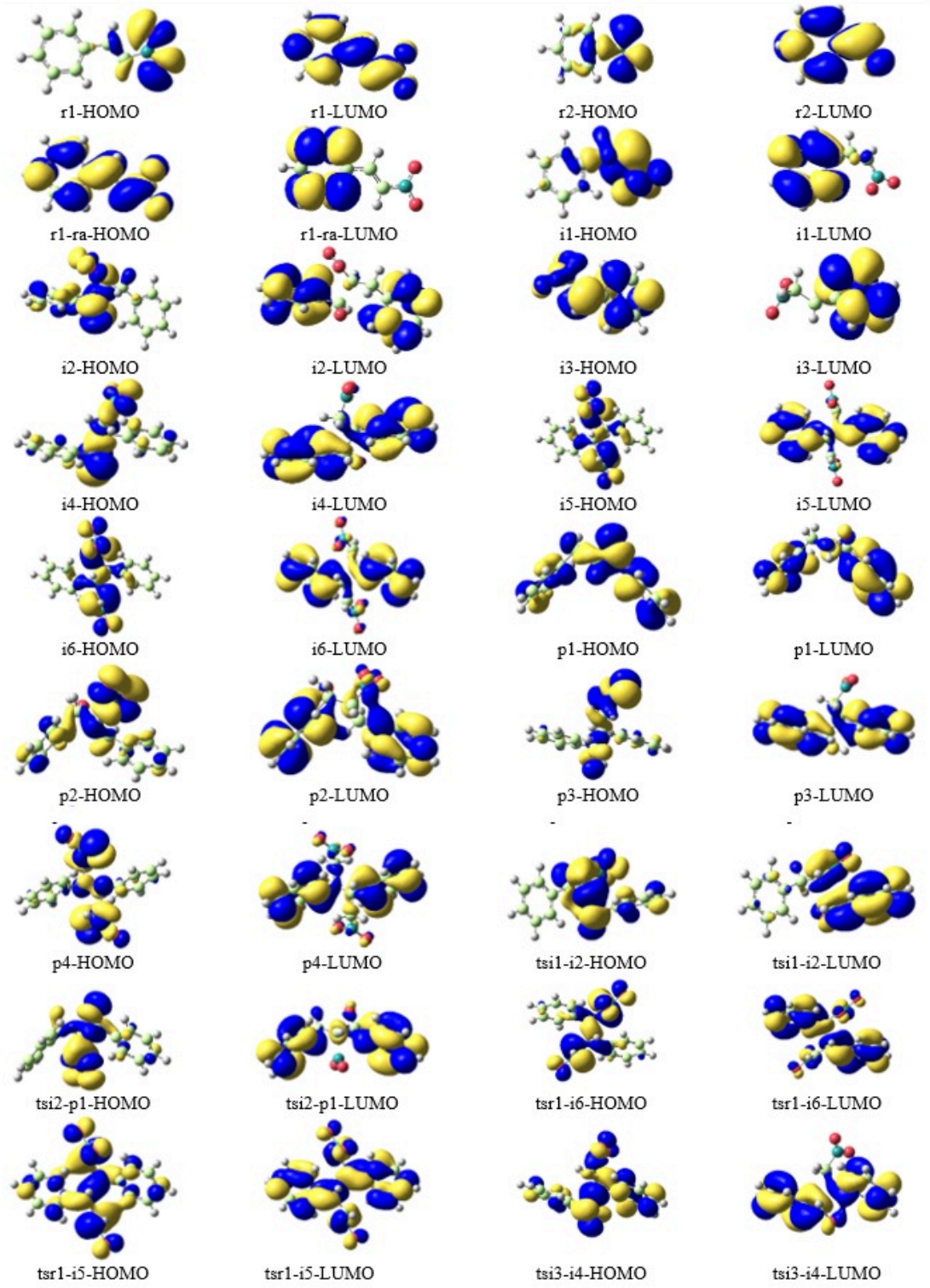

Figure 4

HOMO and LUMO orbitals of all species

Supplementary Files

This is a list of supplementary files associated with this preprint. Click to download.

- Scheme1.png
- Scheme2.png
- Scheme3.png
- Scheme4.png